Terahertz-Driven Luminescence and Colossal Stark Effect in CdSe–CdS Colloidal Quantum Dots

NANO LETTERS

Letter

pubs.acs.org/NanoLett

Terahertz-Driven Luminescence and Colossal Stark Effect in CdSe–CdS Colloidal Quantum Dots

Brandt C. Pein,*[,†] Wendi Chang,[†] Harold Y. Hwang,[‡] Jennifer Scherer,[†] Igor Coropceanu,[†] Xiaoguang Zhao,[§] Xin Zhang,[§] Vladimir Bulović,[†] Moungi Bawendi,[†] and Keith A. Nelson[†]

[†]Department of Chemistry and Department of Electrical Engineering and Computer Science, Massachusetts Institute of Technology, Cambridge, Massachusetts 02139, United States

[‡]Massachusetts Institute of Technology Lincoln Laboratory, Lexington, Massachusetts 02420, United States

[§]Department of Mechanical Engineering, Boston University, Boston, Massachusetts 02215, United States

Supporting Information

ABSTRACT: Optical properties of colloidal semiconductor quantum dots (QDs), arising from quantum mechanical confinement of charge, present a versatile testbed for the study of how high electric fields affect the electronic structure of nanostructured solids. Studies of quasi-DC electric field modulation of QD properties have been limited by electrostatic breakdown processes under high externally applied electric fields, which have restricted the range of modulation of QD properties. In contrast, here we drive CdSe–CdS core–shell QD films with high-field THz-frequency electromagnetic pulses whose duration is only a few picoseconds. Surprisingly, in response to the THz excitation, we observe QD luminescence even in the absence of an external charge source. Our experiments show that QD luminescence is associated with a remarkably high and rapid modulation of the QD bandgap, which changes by more than 0.5 eV (corresponding to 25% of the unperturbed bandgap energy). We show that these colossal energy shifts can be explained by the quantum confined Stark effect even though we are far outside the regime of small field-induced shifts in electronic energy levels. Our results demonstrate a route to extreme modulation of material properties and to a compact, high-bandwidth THz detector that operates at room temperature.

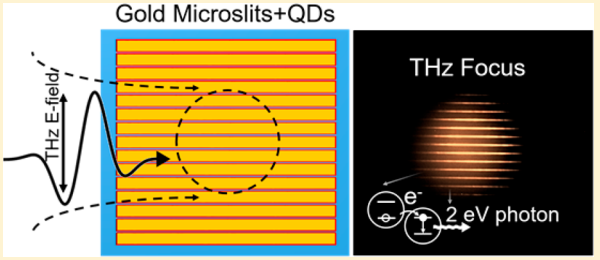

KEYWORDS: *Terahertz, quantum dots, luminescence, Stark effect*

Quantum confinement of charge in QDs is responsible for their tunable electronic and optical properties,[1] which have facilitated the development of QD-based photovoltaics, photodetectors, and light-emitting devices (LEDs). QDs can be actively manipulated with externally applied electric fields,[2−5] providing routes to a new class of multifunctional photonic devices with controllable optical properties. The extent to which those properties can be controlled with extremely large external fields is still largely unexplored, in part because of dielectric breakdown that occurs under quasi-DC fields typically in the 1−10 MV/cm range.

Recent studies demonstrated nonequilibrium responses of material properties driven by intense THz-frequency radiation, including solid−solid phase transitions,[6] impact ionization,[7−9] and field ionization.[10] In many cases, free-space THz field levels that can reach about 1 MV/cm when focused have been enhanced by concentrating THz radiation into subwavelength metallic structures such as split ring resonators and antennas,[6,10−12] allowing access to multi-MV/cm field strengths for nonlinear THz spectroscopy applications. Damage that appears to be dielectric breakdown can be induced by such fields,[13] but the threshold is generally higher than that for quasi-DC fields.

Through the quantum confined stark effect (QCSE), Hoffman et al. previously demonstrated the modulation QD optical absorption using free-space THz electric fields reaching 220 kV/cm suggesting a new method for coherent THz-to-optical detection encoding.[5] Inspired by their work, we applied field enhancement techniques to study the manipulation of QD film optical properties on a picosecond time scale. The results provide fundamental insight into strong-field effects on QD electronic responses and demonstrate, as suggested by Hoffman et al., a pathway to optimize the interaction of THz frequency low switching fields for electro-optic modulation. Moreover we show that enhanced THz electric fields are capable of driving a luminescent response at visible light wavelengths via interdot charge transfer.

To concentrate the incident THz radiation, we use a simple field enhancement structure (FES) design, a metal microslit array on a SiO_2 substrate, consisting of parallel gold lines with 98 μm widths, separated by 2 μm capacitive gaps. This FES offers field enhancement factors intermediate between dipole

Received: May 2, 2017
Revised: August 7, 2017
Published: August 8, 2017

DOI: 10.1021/acs.nanolett.7b01837
Nano Lett. 2017, 17, 5375−5380

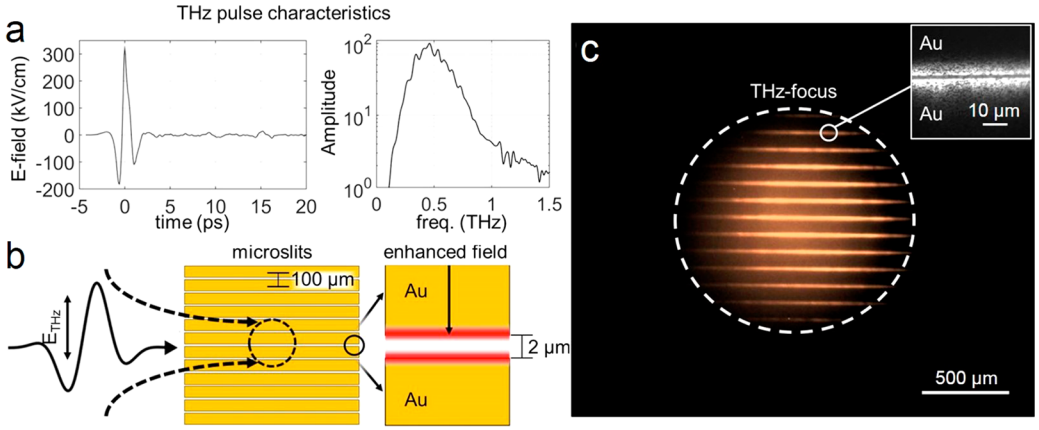

Figure 1. THz field-enhancing microslits and QD luminescence. (a) Incident free-space single-cycle THz pulses have a maximum 320 kV/cm electric field and a spectrum centered at 0.5 THz. (b) Microslit array consisting of parallel horizontal gold lines on an amorphous silica substrate was irradiated by vertically polarized THz pulses. The THz field was enhanced in the 2 μm capacitive gaps between the gold lines. Quantum dots were deposited over the structure, and the QDs in the gap regions were subjected to the enhanced fields. Samples I and II were fabricated respectively without and with a 65 ± 15 nm oxide layer deposited over the structure prior to the QDs. (c) Focusing THz pulses onto either sample I or II generates a visible light image. The image shown is from sample II. The light originates from QD THz-L coming from within the microslit gaps. The inset shows an enlarged image of one gap region, showing that the THz-L is most intense from the regions near the edges of the gaps.

antennas and nanoslit arrays.[14−16] A THz field polarized perpendicular to the gold lines (Figure 1a) is directed onto the microslit array (Figure 1b) and undergoes enhancement of up to 2 orders of magnitude (discussed further below) in the capacitive gaps. QDs deposited over the microslit array are therefore subjected to the enhanced THz field levels. Two samples were tested: sample I consists of QDs on top of bare gold microslits, and sample II has QDs on top of a 65 ± 15 nm silica layer that electrically insulates the QDs from the gold microslits. (See Supporting Information for details of the experimental apparatus and samples.)

Figure 1c shows a visible light image of THz-driven luminescence (THz-L) originating from QDs within the FES gaps of sample II. The inset shows an enlargement of a single gap, indicating that THz-L is enhanced in the vicinity of the gaps. Figure 2 shows the spectral and kinetic characteristics of the THz-L along with photoluminescence (PL) induced by 400 nm wavelength light. The THz-L central wavelength is 620 nm (2.0 eV photon energy; see Figure 2a). Depending on the incident peak field strength, the THz-L spectra fwhm are broadened by as much as 16 meV and red-shifted up to 12 meV relative to the PL spectrum (Figure 2a). The time-dependent PL from both samples could be fit to a monoexponential decay with a 15 ns lifetime (Figure 2b). In contrast, the THz-L emission at all incident field strengths exhibits multiexponential decay with shorter lifetime components than those observed in the PL decay. We ascribe this difference to QD charging under THz excitation. Excitons in charged QDs have additional nonradiative pathways, such as Auger recombination, which can reduce the observed radiative lifetime.[2,17] The presence of local electric fields due to QD charging would also explain the observed red-shift and broadening of the THz-L spectra.

Exciton formation in QD-LEDs driven by DC and quasi-DC electric fields requires long-range transport of electrons and holes. Given the picosecond period of a THz pulse and the low charge carrier mobility of QD films [10^{-4} to 1 cm^2/(V s)], the long-range transport of electrons and holes across a microslit gap is unlikely.[18−20] With our largest incident THz field strength of 320 kV/cm, the peak field across most of the gap region is approximately 2 MV/cm. (As discussed below, the peak field near the edges of the gaps, from where the THz-L emerges, reaches approximately 15 MV/cm, but charge transport across the gap would depend on the field strength in the center.) With a mobility of 1 cm^2/(V s) and a 2 MV/cm electric field, a 1 ps charge could travel a distance of 20 nm, a negligible fraction of the microslit gap width. Due to the limitations imposed by the RC delay in a typical electrically driven capacitive QD-LED structure, earlier a.c.-driven luminescence measurements have been limited to frequencies up to 1 MHz, which is slow enough to allow charge migration between electrodes.[21−24] It is clear that this cannot happen in THz-L. However, even in the absence of long-range migration, an electrode-driven mechanism for THz-L is possible[25−27] in which the alternate polarities of an a.c. field could inject electrons and holes into the conduction and valence bands (CB and VB) respectively of a QD located next to one electrode.

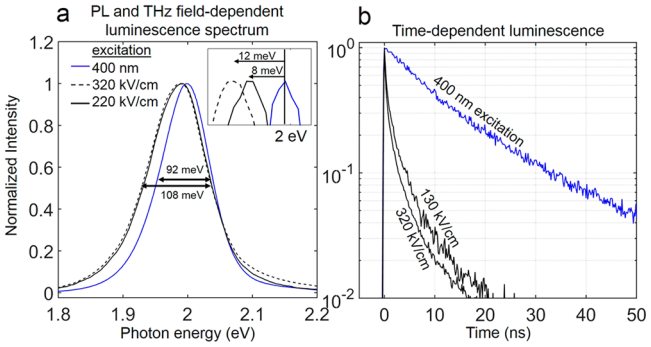

Figure 2. Characteristics of THz-induced luminescence and optically induced photoluminescence originating from microslit samples. (a) The PL spectrum (blue curve) generated by λ = 400 nm excitation wavelength is centered at 2.0 eV. The THz-driven luminescence spectrum is broadened relative to the λ = 400 nm excited spectrum. (Inset) The peak wavelength of THz-driven THz-L emission is red-shifted by as much as 12 meV at the highest incident THz peak field compared to PL emission. (b) Following excitation of the sample with λ = 400 nm pulses, the time-dependent photoluminescence follows a single exponential decay with a 15 ns lifetime. Excitation with 320 kV/cm or 130 kV/cm peak incident THz field generates luminescence with a faster multiexponential decay.

DOI: 10.1021/acs.nanolett.7b01837
Nano Lett. 2017, 17, 5375−5380

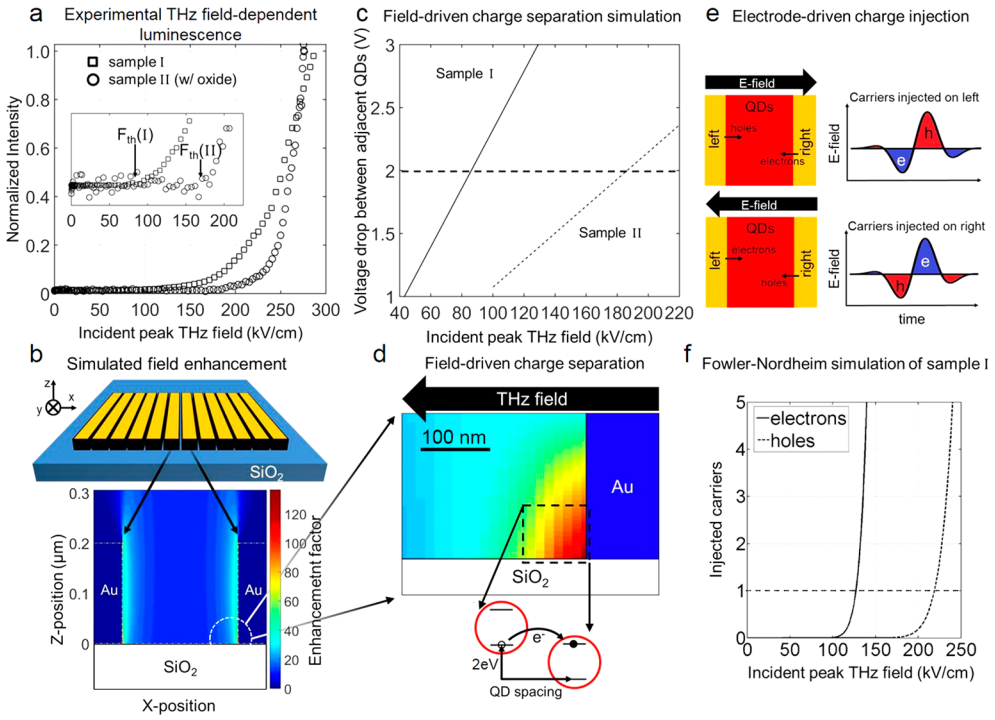

Figure 3. Experimental and simulated threshold THz field required to generate luminescence. (a) THz field-dependent luminescence of CdSe:CdS QDs. Varying the incident peak THz field from 0 to 320 kV/cm generates luminescence with a nonlinear dependence. The threshold F_{th} to generate luminescence occurs at 85 ± 5 kV/cm in sample I and 180 ± 7 kV/cm in sample II. (b) Simulation of microslit THz near-field enhancement. The enhancement has a spatial variation along the x and z positions and is invariant along y. (c) Simulated voltage drop between adjacent QDs as a function of peak incident THz field. The predicted threshold incident THz fields are 86 and 186 kV/cm for samples I and II, respectively, which is in good agreement with experimental values. (d) In the field-driven model, when the voltage drop between QDs is equal to or greater than the QD band gap energy (divided by the electron charge), QD excitons can be generated, leading to luminescence. (e) The electrode-driven charge injection model. During the two half-cycles of the THz field, electrons and holes are injected into QDs adjacent to the electrodes, resulting in exciton formation and luminescence. Due to the different THz field amplitudes in the two polarities, at each electrode more carriers of one type than the other will be injected. (f) Using the Fowler−Nordheim model, the number of injected electrons and holes at the inner face of one side of a slit are computed (by symmetry the opposite side will give the same result with electrons and holes reversed). Since exciton generation requires both electrons and holes, the threshold for THz-L will be determined by the higher of the two thresholds for charge injection (holes for one side, electrons for the other). The onset of THz-L is predicted to begin at 219 kV/cm which is much higher than the experimental result for sample I.

Alternatively, a purely field-driven[24,28,29] mechanism, based on local QD-to-QD charge exchange, could occur. When the voltage drop between neighboring QDs is equal to or greater than the QD band gap, VB electrons can tunnel into the CBs of neighboring QDs leading to a population of electrons and holes which when paired in a QD lead to exciton formation and luminescence. To explore the likelihood of these mechanisms we next analyze the THz-field-dependent luminescence intensity.

The THz-L intensity is a strongly nonlinear function of the peak incident THz field strength (Figure 3a). Below a threshold field level F_{th} of 85 ± 5 kV/cm for sample I and 180 ± 7 kV/cm for sample II, no emission occurs. The THz-L signals near F_{th} are assumed to originate from QDs residing in regions with the strongest field enhancement and for sample II the threshold is predicted to be larger as the QDs are further separated from the gold microslit surface due to the added silica layer. We modeled the spatial variation of the THz electric field in the microslit structures, using Computer Simulation Technology (CST) microwave studio.[30] Based on the peak time-dependent field values, we calculated the field enhancement factor β as a function of the lateral position x within or near a gap (x is also the incident field polarization direction), and the height z above the SiO_2 substrate (Figure 3b). For a given height, z, above the substrate, the change in electric potential ΔV along x from one gold surface toward the other is computed as

$$\Delta V(x, z) = \int_0^x \frac{\beta(x - x', z) F_{\mathrm{THz}}}{\varepsilon_{\mathrm{film}}} \mathrm{d}x' \quad (1)$$

for an incident THz electric field with peak amplitude F_{THz}. Since the THz field is polarized along the x-direction, we neglect polarization components along z. We use a dielectric constant ε_{film} = 3.0 for the QD film, based on the Maxwell−-Garnett effective medium approximation from previous work on CdSe−CdS QD films.[4,24] We assume that the adjacent center-to-center distance of neighboring QDs is 10 nm, based on TEM images (shown in Supporting Information). The largest calculated voltage drop occurs between QD neighbors situated as close as possible to one of the gold electrodes and the oxide substrate, as shown for sample I in Figure 3d. For these locations the voltage drop along the x-direction as a function of incident peak THz field is shown in Figure 3c. Assuming the field-driven model of exciton generation (Figure 3d), F_{th} is reached when the voltage drop between the neighboring QDs equals the QD bandgap energy (2.0 eV) divided by the electron charge. The simulated F_{th} values are 86 kV/cm and 186 kV/cm for samples I and II, respectively, in

DOI: 10.1021/acs.nanolett.7b01837
Nano Lett. 2017, 17, 5375−5380

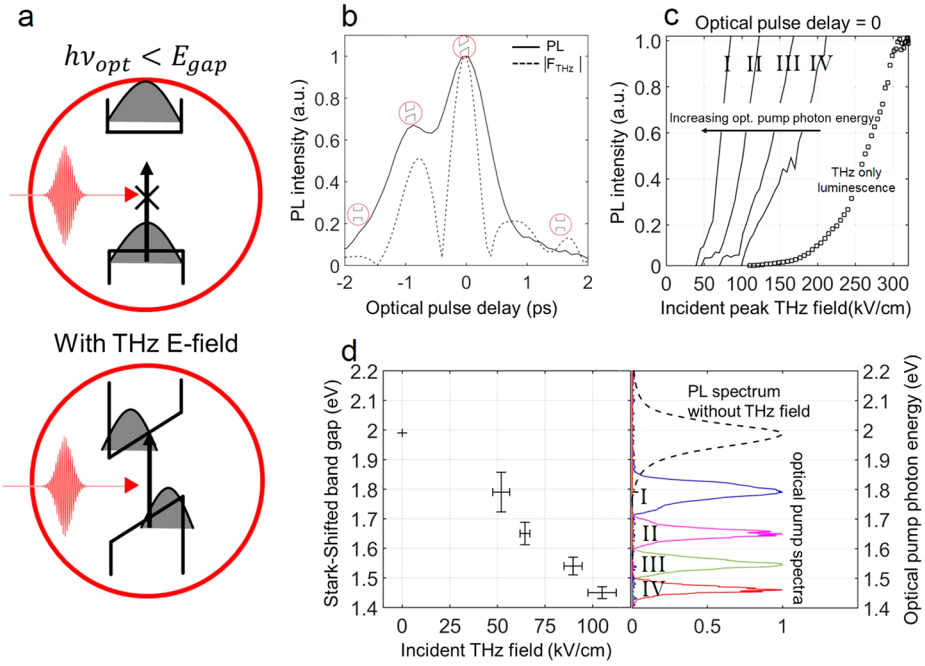

Figure 4. THz field-induced Stark shifting of QDs. (a) Below-band gap photons with energy $h\nu_{opt}$ are not absorbed until a THz field threshold F_{th} is reached which reduces the QD band gap sufficiently, at which point electroabsorption occurs. (b) PL intensity as a function of the time delay between the optical pulse and the THz field peak. The PL intensity generated by the below-bandgap optical photons roughly tracks the absolute value of the THz field. (c) Optical pulse delay is set to 0, and the peak THz field is varied from 0 to 320 kV/cm. When the pump photon energy (indicated by numerals corresponding to spectra in d is increased, the threshold THz field required to generate a PL signal is decreased. At these threshold THz fields, the effective band gap of the QDs has been lowered to equal the optical pulse photon energy. (d) THz field-induced Stark shifting of QDs. (right) The optical pump pulse spectra with the photon energy plotted on the *y*-axis. (left) As the THz field strength is increased, optical pulses with lower photon energy are absorbed and generate PL. The points indicate the threshold field levels (from c) at which the band gap is lowered to an energy equal to the optical photon energy. For a 100 kV/cm incident THz field, the band gap is Stark-shifted by >0.5 eV.

agreement with the experimental values of 85 ± 5 kV/cm and 180 ± 7 kV/cm, respectively.

We note that, in sample I, electrode-driven carrier injection into the QD film is possible in which case the onset of THz-L would occur when carriers begin tunneling into the QD layer from the gold microslits (Figure 3e). Here we compare our results to the Fowler–Nordheim charge tunneling model used in previous works concerning charge injection into low-mobility semiconductors and THz-driven field emission from gold microstructures.[10,31,32] Charges injected into low-mobility semiconducting materials localize at the interface and backflow into the source of the carriers due to thermionic emission, resulting in a net low interfacial current density. Although the enhanced THz field can be strong, the picosecond oscillation period limits the total number of carriers that can be injected per pulse. The Fowler–Nordheim equation for interfacial current density is

$$J_{FN} = a\left(\frac{F_{THz}\beta}{\varepsilon_{film}}\right)^2 \varphi^{-1} \exp\left(\frac{-\varepsilon_{film} b\varphi^{3/2}}{\beta F_{THz}}\right) \quad (2)$$

where $a = 1.53 \times 10^{-6}$ A·eV·V^{-2} and $b = 6.83 \times 10^{9}$ eV$^{-3/2}$·V/m are combinations of universal constants.[33] The average field enhancement nearest to the surfaces of the gold microslits residing within the gaps is $\beta = 106$. The barrier that electrons or holes must overcome to be injected into the QD film is φ, which can take on a range of values depending on the nature of the QD/gold interface. We assume that the Fermi level of the gold microslits lies in the middle of the QD band gap, giving an estimated barrier of 1.0 eV for electrons and holes. Due to the time-dependent THz electric field asymmetry with respect to the troughs and peaks of the field (Figure 3e), there are different field dependencies for electrons and holes on both sides of a gap. Thus, on one side of a gap, more electrons will be injected than holes, and on the opposite side, more holes will be injected than electrons. Integrating J_{FN} over the THz field temporal profile and the slit surface area gives the number of electrons or holes injected within a slit gap for a given peak incident THz field (Figure 3f; see Supporting Information for details on calculations). One electron–hole pair is required to form an exciton, so the threshold incident peak field is predicted to be 219 kV/cm, which is significantly higher than the experimental result for sample I. We therefore conclude that THz-L is, at least at lower incident THz field amplitudes, primarily due to field-driven QD–QD interactions in both samples.

At the highest incident THz field amplitudes, regions of the QD layer can experience electric fields as large as 15 MV/cm on the picosecond time scale. This can have a significant impact on the optical absorption properties due to the QCSE in which an electric field distorts the QD potential energy surface leading to a band gap reduction (Figure 4a). To probe this electroabsorption effect, femtosecond optical pulses with photon energies between 1.45 and 1.8 eV (below the QD bandgap of 2.0 eV) were spatiotemporally overlapped with the THz pulses on the microslit structures.

The optical pulses induce no detectable PL by themselves or when they arrive before or after THz pulses. However, when an optical pulse (with either polarization) is time-coincident with a peak of the THz field, it induces emission, as expected with

DOI: 10.1021/acs.nanolett.7b01837
Nano Lett. 2017, 17, 5375–5380

THz-field-induced electroabsorption. Notably, as the optical pulse is variably delayed across the THz pulse field temporal profile, it generates a PL signal whose intensity approximately tracks the absolute magnitude of the THz field (Figure 4b) which is consistent with Hoffmann et al.'s previously demonstrated THz-field-induced electroabsorption experiments performed on InGaAs/GaAs QDs.[5] For the data in Figure 4c, we fixed the optical excitation pulses at zero delay (relative to the THz field peak) and varied the THz field amplitude to determine the F_{th} value for electroabsorption. The measurement was repeated for different incident optical pump photon energies. As the optical pump photon energy was increased, F_{th} was reduced, again consistent with THz-field-induced electroabsorption. At each threshold field level, the QD band gap energy is reduced from its field-free value to the optical pump photon energy (Figure 4d). For a 100 kV/cm incident THz field (near the onset of THz-L), the band gap is reduced by more than 0.5 eV which is an order of magnitude larger than previously demonstrated giant Stark effect measurements of QDs.[3] At higher incident fields the QD band gap is likely reduced further, but the overlap of electroabsorption-enhanced luminescence with purely THz-driven luminescence signals complicates quantitative determination of the additional bandgap reduction.

This work demonstrates that ultrafast THz pulses can drive a luminescence response in a colloidal QD film. While electrode-driven charge injection and purely field-driven mechanisms can both contribute to THz-L, our results indicate that the field-driven mechanism dominates even when charge injection is possible. THz-L is driven by direct field-induced distortion of the QD electronic structure. We observe a modulation of the QD bandgap of more than 0.5 eV, shifting the QD absorption across a significant part of the visible spectrum. The QD emission and spectral shifting driven by the THz field may be used as a novel approach to THz detection and imaging and for ultrahigh-frequency electro-optic modulation.

■ ASSOCIATED CONTENT

Supporting Information

The Supporting Information is available free of charge on the ACS Publications website at DOI: 10.1021/acs.nanolett.7b01837.

Description of the experimental apparatus and generation of ultrafast terahertz pulses. Details of quantum dot synthesis and characterization. Microslit characterization including fabrication and electromagnetic simulations. Explanation of microslit-to-quantum dot carrier injection model (PDF)

■ AUTHOR INFORMATION

Corresponding Author

*E-mail: bpein@mit.edu. Phone: 617-253-1956.

ORCID

Brandt C. Pein: 0000-0002-6145-1361

Moungi Bawendi: 0000-0003-2220-4365

Author Contributions

B.C.P., H.Y.H., and K.A.N. conceived the study. I.C. and J.S. synthesized and characterized the QDs used in the experiments. H.Y.H., X. Zhao, and X. Zhang fabricated the microslit field enhancement structures. H.Y.H. performed the electromagnetic simulations of the microslit field enhancement structures, while B.C.P. and W.C. interpreted and utilized these results for charge injection and separation simulations. B.C.P. and W.C. collected all spectroscopic data from the THz field dependent luminescence and stark shifting experiments as well as the experimental images of THz driven luminescence. B.C.P. prepared the manuscript with the assistance of W.C., H.Y.H, V.B., and K.A.N. All authors read and commented on the manuscript.

Notes

The authors declare no competing financial interest.

■ ACKNOWLEDGMENTS

W.C., V.B., J.S., I.C., M.B., and K.A.N. were supported as part of the Center for Excitonics, an Energy Frontier Research Center funded by the US Department of Energy, Office of Science, Office of Basic Energy Sciences under Award Number DE-C0001088. H.Y.H. and B.P. were supported by Office of Naval Research grants no. N00014-13-1-0509 and N00014-16-1-2090. Equipment for the project was provided by Office of Naval Research grant no. N00014-15-1-2879.

■ ABBREVIATIONS

QD, quantum dot; LED, light-emitting device; THz, terahertz; FES, field enhancement structure; THz-L, terahertz-driven luminescence; MHz, megahertz; CB, conduction band; VB, valence band; CST, computer simulation technology; PL, photoluminescence

■ REFERENCES

(1) Brus, L. E. *J. Chem. Phys.* **1984**, *80*, 4403.

(2) Empedocles, S. A. *Science* **1997**, *278*, 2114−2117.

(3) Bennett, A. J.; Patel, R. B.; Skiba-Szymanska, J.; Nicoll, C. A.; Farrer, I.; Ritchie, D. A.; Shields, A. J. *Appl. Phys. Lett.* **2010**, *97*, 031104.

(4) Bozyigit, D.; Yarema, O.; Wood, V. *Adv. Funct. Mater.* **2013**, *23*, 3024−3029.

(5) Hoffmann, M. C.; Monozon, B. S.; Livshits, D.; Rafailov, E. U.; Turchinovich, D. *Appl. Phys. Lett.* **2010**, *97*, 231108.

(6) Liu, M.; Hwang, H. Y.; Tao, H.; Strikwerda, A. C.; Fan, K.; Keiser, G. R.; Sternbach, A. J.; West, K. G.; Kittiwatanakul, S.; Lu, J.; Wolf, S. A.; Omenetto, F. G.; Zhang, X.; Nelson, K. A.; Averitt, R. D. *Nature* **2012**, *487*, 345−348.

(7) Hoffmann, M. C.; Hebling, J.; Hwang, H. Y.; Yeh, K.-L.; Nelson, K. A. *Phys. Rev. B: Condens. Matter Mater. Phys.* **2009**, *79*, 161201.

(8) Hirori, H.; Shinokita, K.; Shirai, M.; Tani, S.; Kadoya, Y.; Tanaka, K. *Nat. Commun.* **2011**, *2*, 594.

(9) Lange, C.; Maag, T.; Hohenleutner, M.; Baierl, S.; Schubert, O.; Edwards, E. R. J.; Bougeard, D.; Woltersdorf, G.; Huber, R. *Phys. Rev. Lett.* **2014**, *113*, 227401.

(10) Iwaszczuk, K.; Zalkovskij, M.; Strikwerda, A. C.; Jepsen, P. U. *Optica* **2015**, *2*, 116.

(11) Fan, K.; Hwang, H. Y.; Liu, M.; Strikwerda, A. C.; Sternbach, A.; Zhang, J.; Zhao, X.; Zhang, X.; Nelson, K. A.; Averitt, R. D. *Phys. Rev. Lett.* **2013**, *110*, 217404.

(12) Tarekegne, A. T.; Iwaszczuk, K.; Zalkovskij, M.; Strikwerda, A. C.; Jepsen, P. U. *New J. Phys.* **2015**, *17*, 043002.

(13) Hwang, H. Y.; Fleischer, S.; Brandt, N. C.; Perkins, B. G.; Liu, M.; Fan, K.; Sternbach, A.; Zhang, X.; Averitt, R. D.; Nelson, K. A. *J. Mod. Opt.* **2015**, *62*, 1447−1479.

(14) Seo, M. A.; Park, H. R.; Koo, S. M.; Park, D. J.; Kang, J. H.; Suwal, O. K.; Choi, S. S.; Planken, P. C. M.; Park, G. S.; Park, N. K.; Park, Q. H.; Kim, D. S. *Nat. Photonics* **2009**, *3*, 152−156.

(15) Lee, K. G.; Park, Q.-H. *Phys. Rev. Lett.* **2005**, *95*, 103902.

(16) Shalaby, M.; Fabiańska, J.; Peccianti, M.; Ozturk, Y.; Vidal, F.; Sigg, H.; Morandotti, R.; Feurer, T. *Appl. Phys. Lett.* **2014**, *104*, 171115.

DOI: 10.1021/acs.nanolett.7b01837
Nano Lett. 2017, 17, 5375−5380

(17) Caruge, J. M.; Halpert, J. E.; Wood, V.; Bulović, V.; Bawendi, M. G. *Nat. Photonics* **2008**, *2*, 247−250.
(18) Ginger, D. S.; Greenham, N. C. *J. Appl. Phys.* **2000**, *87*, 1361.
(19) Yu, D.; Wang, C.; Guyot-Sionnest, P. *Science* **2003**, *300*, 1277−1280.
(20) Talapin, D. V.; Murray, C. B. *Science* **2005**, *310*, 86−89.
(21) Wood, V.; Halpert, J. E.; Panzer, M. J.; Bawendi, M. G.; Bulović, V. *Nano Lett.* **2009**, *9*, 2367−2371.
(22) Mu, W.; Zhang, P.; Xu, J.; Sun, S.; Xu, J.; Li, W.; Chen, K. *IEEE J. Sel. Top. Quantum Electron.* **2014**, *20*, 206−211.
(23) Cho, S. H.; Sung, J.; Hwang, I.; Kim, R. H.; Choi, Y. S.; Jo, S. S.; Lee, T. W.; Park, C. *Adv. Mater.* **2012**, *24*, 4540−4546.
(24) Bozyigit, D.; Wood, V.; Shirasaki, Y.; Bulovic, V. *J. Appl. Phys.* **2012**, *111*, 113701.
(25) Tavares, L.; Kjelstrup-Hansen, J.; Rubahn, H.-G. *Nanotechnology* **2012**, *23*, 425203.
(26) Liu, X.; Wallmann, I.; Boudinov, H.; Kjelstrup-Hansen, J.; Schiek, M.; Lützen, A.; Rubahn, H.-G. *Org. Electron.* **2010**, *11*, 1096−1102.
(27) Yamao, T.; Shimizu, Y.; Terasaki, K.; Hotta, S. *Adv. Mater.* **2008**, *20*, 4109−4112.
(28) Wood, V.; Panzer, M. J.; Bozyigit, D.; Shirasaki, Y.; Rousseau, I.; Geyer, S.; Bawendi, M. G.; Bulović, V. *Nano Lett.* **2011**, *11*, 2927−2932.
(29) Wood, V.; Panzer, M. J.; Caruge, J.-M.; Halpert, J. E.; Bawendi, M. G.; Bulović, V. *Nano Lett.* **2010**, *10*, 24−29.
(30) CST—Computer Simulation Technology. www.cst.com/products/cstmws (accessed Aug 8, 2017).
(31) Davids, P. S.; Kogan, S. M.; Parker, I. D.; Smith, D. L. *Appl. Phys. Lett.* **1996**, *69*, 2270.
(32) Parker, I. D. *J. Appl. Phys.* **1994**, *75*, 1656.
(33) Fowler, R. H.; Nordheim, L. *Proc. R. Soc. London, Ser. A* **1928**, *119*, 173−181.

DOI: 10.1021/acs.nanolett.7b01837
Nano Lett. 2017, 17, 5375−5380